An estimate of strong local body forcing and gravity wave radiation based on OH airglow and meteor radar observations

David C. Fritts and Sharon L. Vadas

NorthWest Research Associates, CoRA Division, Boulder, CO, USA

Yoshinori Yamada

Department of Geophysics, Tohoku University, Sendai, Japan

[1] Airglow measurements of gravity wave and smaller-scale flow features, used together with other measurements of larger-scale winds, provide a unique ability to quantify gravity wave dynamics at mesopause altitudes. We consider here an event observed with an OH airglow imager and the meteor radar at the MU Observatory in Japan. This was a wave breaking event of unusually large amplitude and momentum flux. Our hypothesis is that such events are relatively common, and that the resulting local forcing of the mean flow represents a vigorous source of secondary gravity waves that penetrate well into the thermosphere. Our analysis suggests a gravity wave momentum flux of ~ 900 m^{2}s^{-2}, far larger than estimated by other techniques, and a mean flow acceleration of ~ 80 ms^{-1} in less than an hour. We also estimate the scales and frequencies of the secondary waves resulting from this local body forcing. *INDEX TERMS:* 3334 Meteorology and Atmospheric Dynamics: Middle atmospheric dynamics (0341, 034); 3369 Thermospheric dynamics; 3384 Waves and tides

1. Introduction

[2] Airglow measurement techniques now have an ability to define not just the larger gravity wave structures modulating airglow emissions, but also gravity wave momentum fluxes and smaller-scale flow features suggestive of wave instability dynamics [*Swenson and Mende*, 1994]. Radar and lidar techniques, in contrast, provide estimates of gravity wave amplitudes, frequencies, vertical structures, and fluxes averaged over some time interval, typically at least an hour [*Fritts and Vincent*, 1987], but little or no information on horizontal scales. As a result, an increasing number of observations are merging airglow and radar or lidar measurements of small-scale gravity waves and large-scale winds and temperatures to provide a more quantitative picture of intrinsic wave properties [*Taylor et al.*, 1995; *Isler et al.*, 1997; *Hecht et al.*, 1997; *Walterscheid et al.*, 1999; *Yamada et al.*, 2001]. A unique ability of airglow instrumentation in these applications is the potential to define the spatial scales of gravity waves and instabilities and, equally importantly, the spatial extents of the wave packets.

[3] On the theoretical side, recent studies by *Vadas and Fritts* [2001] and *Vadas et al.* [2002] have called attention to the potential for localized gravity wave forcing to result in significant radiation of secondary waves having properties that may enable their propagation to very high altitudes. If such forcing can be documented, it suggests a potential for gravity wave transports of momentum and energy to play a role in thermospheric dynamics to much higher altitudes than previously believed important.

[4] Our purposes in this paper are twofold. We first estimate in section 2 the magnitude of gravity wave forcing accompanying the wave breaking event described by *Yamada et al.* [2001], as this

appears to be an exceptionally strong forcing event. As such, it highlights the potential for mean gravity wave forcing being composed of a series of sporadic forcing events rather than the nearly constant forcing often assumed in large-scale models and middle atmosphere GCMs. We also estimate the spatial and temporal scales on which this gravity wave forcing occurs. These estimates are used in section 3 to anticipate the scales of secondary waves generated through local body forcing and their potential for propagation to higher altitudes. A discussion and our conclusions are offered in sections 4 and 5.

2. Gravity Wave Amplitudes and Fluxes Inferred From Airglow and Radar

[5] *Yamada et al.* [2001] performed a careful analysis of a gravity wave event occurring on 23 December 1995 above the MU Observatory. The primary gravity wave was found to have a horizontal wavelength of ~ 27 km, a direction of propagation towards the SW, largely opposed to the large-scale flow (from the NNE), an intrinsic phase speed of ~ 80 ms^{-1} at the OH airglow layer prior to the occurrence of wave breaking and instability structures in the OH data, and a decreasing phase speed accompanying wave instability and thereafter (see their Figures 1 to 3). *Yamada et al.* [2001] also inferred gravity wave properties from 1400 to 1800 UT, though the duration of very large amplitudes appears to have spanned a much shorter interval, ~ 1630 to 1650 UT. The corresponding evolution of the large-scale wind field along the direction of gravity wave propagation, not shown by *Yamada et al.* [2001], but reproduced as Figure 1 here, showed wind accelerations in the direction of wave propagation amounting to ~ 50 ms^{-1} or greater at altitudes of 87 km and above in less than 1 hour.

2.1. Estimation of Gravity Wave Parameters

[6] The intrinsic phase speed of a wave motion represents an upper limit on the horizontal perturbation velocity of the wave based on a convective instability threshold, $u' \sim c - \overline{u}$, where c and $\overline{u}$ are the wave phase speed and the large-scale motion in the direction of wave propagation. A large breaking amplitude also implies a large vertical wavelength, a large instability depth, and large horizontal instability scales, as seen by *Fritts et al.* [1993], *Swenson and Mende* [1994], and *Hecht et al.* [1997]. Smaller-scale instability structures with alignment along rather than normal to wave phase fronts, as seen in Figure 1 of *Yamada et al.* [2001], are more indicative of the lower edge of a turbulent region (see *Fritts et al.* [1998]), with the primary instability occurring at higher altitudes and larger horizontal scales. Thus, the instability accompanying wave breaking observed by *Yamada et al.* [2001] almost certainly was triggered by a decreasing intrinsic phase speed (and increasing $u'/(c - \overline{u})$) in the strong wind shear above the OH airglow layer.

[7] We can quantify our estimate of the wave amplitude further by recognizing that a breaking wave will only introduce turbulence and mixing a short distance (less than a vertical wavelength) below
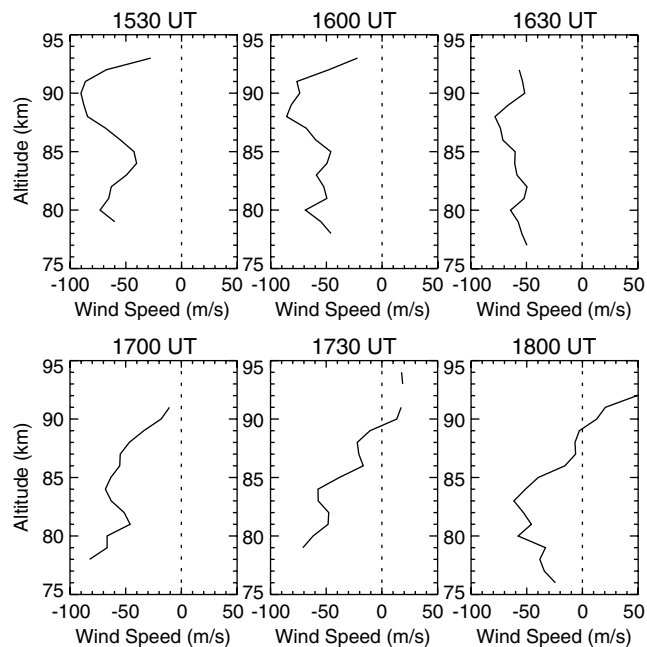
Figure 1. Profiles of horizontal wind speed in the direction of wave propagation obtained with the MU meteor radar from 1530 to 1800 UT on 23 December 1995. Negative values indicate wave propagation opposed to the mean motion.

the altitude at which the wave achieves an unstable amplitude, based on the numerical studies by *Andreassen et al.* [1998] and *Fritts et al.* [1998]. The approximate dispersion relation is $m^2 = N^2/(c - \overline{u})^2 - k^2$, where k and m are the horizontal and vertical wavenumbers of the gravity wave, $N \sim 2 \times 10^{-2} s^{-1}$ is representative of the winter mesosphere, and we have assumed that $m^2 \gg 1/4H^2$ (appropriate for phase speeds ~ 60 ms^{-1} or less). This implies vertical wavelengths of 6.5, 10, 14, 19, and 26 km for intrinsic phase speeds of 20, 30, 40, 50, and 60 ms^{-1}, respectively. Importantly, waves having $u' \sim (c - \overline{u}) \sim 20$ or 30 ms^{-1} would lead to instability only above ~ 93 km, based on the meteor wind profiles prior to 1630 UT (see Figure 1). Such a breaking event would be unlikely to have contributed turbulence and small-scale structure at the airglow layer. Larger wave amplitudes, hence larger intrinsic phase speeds at the breaking altitude, would favor lower and deeper instability structures. This suggests a wave amplitude of ~ 40 to 60 ms^{-1}, and we will focus on this range of amplitudes below. In all cases, wave breaking would occur primarily above the airglow layer, so the small-scale structures in the airglow images likely represent only the lower edge of the turbulent region. As such, they are unlikely to reveal the character of initial instability as suggested by *Yamada et al.* [2001].

[8] With an estimate of u', we can also estimate the vertical perturbation velocity, w', and the wave momentum flux (per unit mass), $\overline{u'w'}$ by employing the dispersion relation and the continuity equation, $ku' = -mw'$. For u' of 40, 50, and 60 ms^{-1}, we obtain vertical velocity estimates of 21, 36, and 58 ms^{-1}, and momentum flux estimates of 420, 900, and 1750 m^{2}s^{-2}, respectively. In support of these estimates, we note that wave intensity variations on the CCD at the peak of this event were $I'/\overline{I} \sim 0.55$, which is much larger than the ~ 3 to 5% intensity variations typically associated with much smaller flux estimates [*Swenson and Liu*, 1998].

[9] By radar measurement or modeling standards, these are enormous velocity and momentum flux estimates. The largest values inferred by radar for short intervals in the mesosphere and lower thermosphere (MLT) are typically ~ 30 to 60 m^{2}s^{-2} [*Fritts and Vincent*, 1987; *Reid et al.*, 1988], and were themselves much

larger than mean values of ~ 5 to 10 m^{2}s^{-2} accounting for the mean wind structure of the MLT. On the other hand, radar measurements are averaged in space and time, and large vertical motions at MLT altitudes are occasionally observed. By contrast, the large amplitude and flux estimates above apply to only a small part of the wave field observed with the OH imager by *Yamada et al.* [2001] and only for a short time. Events having $I'/\overline{I} \sim 0.5$ are quite uncommon, but values of $I'/\overline{I} \sim 0.2$ to 0.3 are relatively more common, based on continuing observations with the instrument used in this study.

[10] Assuming now (1) that this gravity wave experiences a constant amplitude with height (this is a conservative estimate, since the large-scale shear in the direction of propagation suggests a more rapid amplitude decay with height) and (2) that the associated body force is applied over the duration of a wave period (~ 10 min), the impulse applied to the large-scale flow in the direction of wave propagation for a wave amplitude of 50 ms^{-1} is

$$\Delta\overline{u} \simeq \overline{u'w'}\Delta t/H \sim 80 ms^{-1} \qquad (1)$$

over the volume of wave forcing. If wave dissipation is confined by the strong shears at greater altitudes, the momentum flux divergence and forcing would be larger, but over a shallower depth. We note that these estimates are comparable to, or greater than, the large-scale flow accelerations above ~ 87 km at the time of apparent wave instability.

2.2. Estimation of Body Forcing Geometry

[11] Based on the OH imager data presented by *Yamada et al.* [2001], we estimate the horizontal extent of strong forcing to have been $\sim 2\lambda_x$, or ~ 50 km. The vertical extent of the body force is less constrained; however, it is likely greater than the initial distance to the gravity wave critical level ($c = \overline{u}$) because transient, large-amplitude waves experience "self acceleration" and thus smaller decreases in $c - \overline{u}$ than expected on the basis of linear theory [*Fritts and Dunkerton*, 1984; *Sutherland*, 2001]. The vertical extent of the body force is also likely to be less than the initial vertical wavelength at the time of instability, as instability will strongly limit wave amplitude on the time scale of a buoyancy period [*Andreassen et al.*, 1998; *Fritts et al.*, 1998]. These limits suggest a body force depth of ~ 5 to 20 km, with scales ~ 10 km and larger more likely. We also assume a temporal extent of strong forcing of $\sim$ one wave period, or ~ 10 min.

3. Secondary Gravity Wave Scales

[12] It is well known that wave breaking generates secondary waves, but the mechanisms for such generation have yet to be fully explored. One mechanism that has been quantified is that arising from the spatially- and temporally-localized body forces accompanying wave breaking [*Vadas and Fritts*, 2001]. Local body forcing leads to both (1) a balanced mean response that is insensitive to the temporal variability of the forcing and (2) generation of secondary waves that arise as part of the adjustment process. The secondary wave spectrum is determined by both the spatial and temporal character of the body force, with higher-frequency waves arising from deeper, more transient forcings.

[13] Here we explore the secondary wave spectrum that might have arisen from the wave breaking event described by *Yamada et al.* [2001] because of the dramatic nature of this event. To do so, we employ the theoretical formulation by *Vadas and Fritts* [2001] to estimate the spatial and temporal scales of gravity waves arising from the local body force defined above.

[14] For simplicity, we consider a body force centered at $\mathbf{x}_0 = (x_0, y_0, z_0)$ having a Gaussian spatial distribution with amplitude u_0 and half widths at half maximum of σ_x, σ_y, and σ_z, and a temporal variation given by $(1 - \cos 2\pi t/\sigma_t)/\sigma_t$. The formulation by *Vadas et al.* [2002] specifies the secondary wave momentum fluxes

aligned along and perpendicular to the direction of the body forcing. These are given for each wavenumber spectral element by

$$\overline{\tilde{u}_{\parallel}\tilde{w}^*} \simeq -\beta m k^3 \omega^2 \left(N^2 - \omega^2\right) \quad (2)$$

$$\overline{\tilde{u}_{\perp}\tilde{w}^*} \simeq -\beta m k^2 \omega^2 \left(N^2 - \omega^2\right). \quad (3)$$

Here $\tilde{u}_{\parallel}$, $\tilde{u}_{\perp}$, and $\tilde{w}$ are the Fourier transforms of the secondary wave horizontal and vertical velocities, k and l are the secondary wave horizontal wavenumbers parallel and perpendicular to the body force, $\omega = k(c - \overline{u}) = \sqrt{(k^2 + l^2)N^2/(k^2 + l^2 + m^2)}$ is the secondary wave intrinsic frequency, overlines denote a temporal average over the wave period, and asterisks denote a complex conjugate. Additionally,

$$\beta \simeq \left\{ \frac{4a^4 \sin^2(\omega\sigma_t/2)}{(a^2 - \omega^2)^2 \omega^2 \sigma_t^2} \right\} \frac{|\tilde{F}|^2}{2(k^2 + l^2)^2 N^4}, \quad (4)$$

$a = 2\pi/\sigma_t$, $\tilde{F}$ is the Fourier transform of F, and we have neglected rotation since these body forces are deep, i.e., have $\sigma_z/\sigma_{x,y} \gg f/N$. The term in curly brackets in Equation (4) equals one when the forcing duration is short. Readers are referred to *Vadas and Fritts* [2001] for additional details.

4. Discussion

[15] Secondary waves radiate outward in a symmetric cone about the body force, with larger amplitudes and momentum fluxes
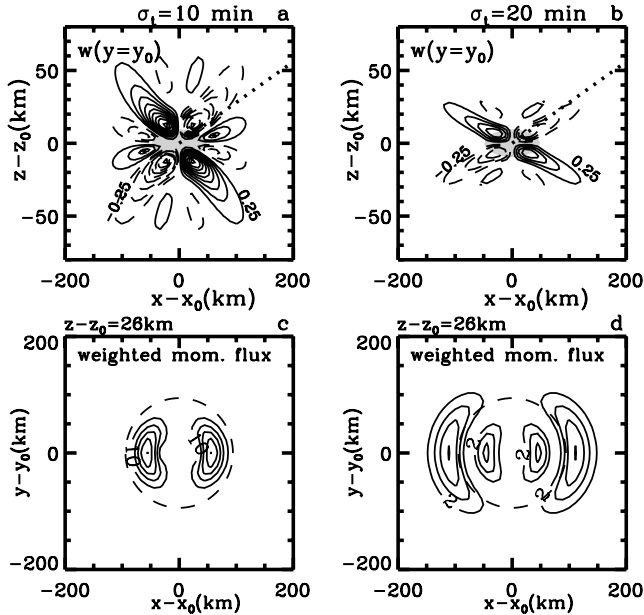

Figure 2. Vertical cross sections of vertical velocity weighted by $\rho^{1/2}$ (a and b) and horizontal cross sections of momentum flux, $\sqrt{(u_{\parallel}w)^2 + (u_{\perp}w)^2}$, at a height 26 km above the center of forcing (c and d) for Gaussian body forcings with $u_0 = 100$ ms^{-1}, 50 km widths, 10 km depths, and $\sigma_t = 10$ (a and c) and 20 min (b and d). Solid (dashed) contours in a and b are positive (negative) w, and dashed lines in c and d denote the intersection of waves having the characteristic frequency and originating at the center of the source with the horizontal surface 26 km above the forcing. Contour intervals are 0.25 ms^{-1} in a and b and 10 and 2 m^{2}s^{-2} in c and d, respectively.

in the direction of the body force than at other azimuths. Vertical velocities (weighted by $\rho^{1/2}$ to display the wave phase structure over extended altitudes) for body forcings with $u_0 = 100$ ms^{-1}, 50 km width, 10 km depth, and $\sigma_t = 10$ and 20 min are shown with vertical cross sections in Figures 2a and b. The momentum fluxes in a horizontal plane 26 km above the forcing centers are shown for each forcing duration in Figures 2c and d; momentum fluxes below the body force are insignificant compared to incident wave fluxes. The two cases exhibit significant differences in secondary wave radiation, despite the same forcing geometry. In both cases, secondary wave scales are determined primarily by the source geometry, but there is significant cancellation of the higher-frequency motions when the force duration is comparable to or exceeds the characteristic period, $T_c = 2\pi/\omega_c$, with $\omega_c \simeq \sqrt{2}\,\sigma_z N/\sigma_x$. Comparison of the two cases reveals that the shorter duration forcing results in waves having higher frequencies, steeper phase propagation, and larger momentum fluxes. For reference, the dotted lines in Figures 2 a and b show the phase slope of waves at the characteristic frequency, ω_c, for which horizontal wave velocities maximize (*Vadas et al.* [2002]). The momentum fluxes likewise reflect the effects of phase cancellation, with the shorter (longer) duration forcing leading to momentum flux maxima at steeper (less steep) phase angles and having larger (smaller) magnitudes. The momentum fluxes per quadrant (i.e., upward and eastward) at the source height and averaged over the source volume for these two cases are 11 and 4 m^{2}s^{-2}, respectively, and reveal a dramatic influence on wave radiation efficiency. For deeper forcing (i.e., a 20 km depth), these differences are even greater, 16 and 5 m^{2}s^{-2}. Because of the quadratic dependence of secondary wave momentum fluxes on forcing amplitude, u_0, [*Vadas and Fritts*, 2001], we expect that the strongest, deepest, and shortest duration forcing events will account for the majority of such radiation.

[16] Figure 3 shows the secondary wave momentum flux spectrum, $\sqrt{(\tilde{u}_{\parallel}\tilde{w})^2 + (\tilde{u}_{\perp}\tilde{w})^2}$, due to secondary waves generated in each quadrant by a horizontal body force of 50 km width for forcing depths of 10 and 20 km and durations of 10 and 20 min. In each case, but especially for the deeper and shorter forcings, secondary waves are generated having large horizontal phase speeds (and large vertical wavelengths). The secondary waves thus have the ability to largely avoid critical level dissipation, and so will propagate and transport significant momentum to very much higher altitudes.

5. Conclusions

[17] We have employed airglow and meteor radar observations of a breaking gravity wave by *Yamada et al.* [2001] to estimate the magnitude of wave forcing and the spatial and temporal scales on which this forcing occurs. The gravity wave was judged to have a very localized response, both spatially and temporally, somewhat above the OH airglow layer, based on intrinsic phase speed and frequency estimates, large-scale wind shears at greater altitudes, and the spatial extent of the gravity wave and the resulting turbulent structures in the OH airglow. The magnitude of the estimated wave forcing was far larger than previous estimates based on radar measurements or modeling studies, ~900 m^{2}s^{-2} (with an uncertainty of ~2). This estimate, however, is consistent with the magnitude and the timing of the large-scale wind accelerations above the airglow layer observed with the meteor radar. Such events also suggest that sporadic, large-amplitude forcing accompanying localized wave breaking may be more the rule than the exception, given the tendency for momentum fluxes to be associated primarily with waves having small horizontal scales and high intrinsic frequencies.

[18] The scales and momentum fluxes of gravity waves generated by the body forcing geometries and magnitudes estimated above were computed using the formulation described by *Vadas*
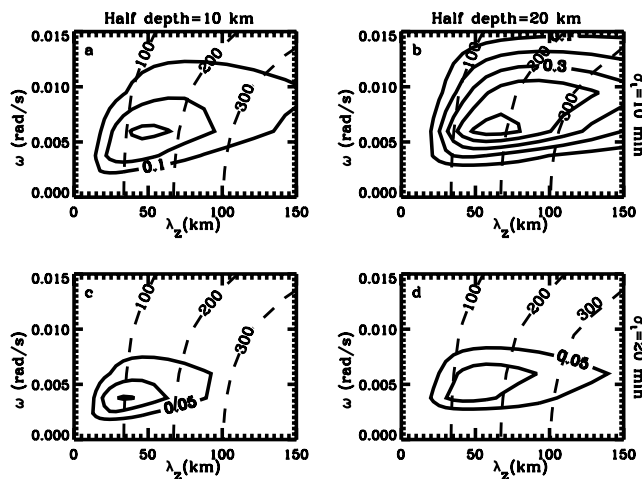
Figure 3. Secondary wave momentum flux spectrum (in λ_z and ω) in each quadrant (i.e., upward and eastward) at the source height and averaged over the source volume generated with $u_0 = 100$ ms^{-1} in the absence of rotation (solid contours). Vertical extents and durations of the forcings are 10 km and 10 min (a), 20 km and 10 min (b), 10 km and 20 min (c), and 20 km and 20 min (d) and contours are in m^{2}s^{-2} (flux content form). Dashed lines indicate horizontal phase speeds in 100 ms^{-1} intervals (with $l = 0$). The integrated momentum fluxes in each quadrant are 11 (a), 16 (b), 4 (c), and 5 m^{2}s^{-2} (d).

and Fritts [2001]. Results suggest the generation of significant secondary waves having scales and phase speeds that may enable their penetration to much higher altitudes. If such variability in gravity wave forcing is common (as we believe), then gravity waves will likely also have a dynamically significant role to much higher altitudes than described by present parameterization schemes.

References

Andreassen, Ø., P. Ø. Hvidsten, D. C. Fritts, and S. Arendt, Vorticity dynamics in a breaking gravity wave, 1. Initial instability evolution, *J. Fluid Mech.*, *367*, 27–46, 1998.

Fritts, D. C., and T. J. Dunkerton, A quasi-linear study of gravity wave saturation and self-acceleration, *J. Atmos. Sci.*, *41*, 3272–3288, 1984.

Fritts, D. C., and R. A. Vincent, Mesospheric momentum flux studies at Adelaide, Australia: Observations and a gravity wave/tidal interaction model, *J. atmos. Sci.*, *44*, 605–619, 1987.

Fritts, D. C., J. R. Isler, G. E. Thomas, and Ø. Andreassen, Wave breaking signatures in noctilucent clouds, *Geophys. Res. Lett.*, *20*, 2039–2042, 1993.

Fritts, D. C., S. Arendt, and Ø. Andreassen, Vorticity dynamics in a breaking internal gravity wave, 2. Vortex interactions and transition to turbulence, *J. Fluid Mech.*, *367*, 47–65, 1998.

Hecht, J. H., R. L. Walterscheid, D. C. Fritts, J. R. Isler, D. C. Senft, C. S. Gardner, and S. J. Franke, Wave breaking signatures in OH airglow and sodium densities and temperatures, Part I: Airglow imaging, Na lidar, and MF radar observations, *J. Geophys. Res.*, *102*, 6655–6668, 1997.

Isler, J. R., M. J. Taylor, and D. C. Fritts, Observational evidence of wave ducting in the mesosphere, *J. Geophys. Res.*, *102*, 26,301–26,313, 1997.

Reid, I. M., R. Rüster, P. Czechowsky, and G. Schmidt, VHF radar measurements of momentum flux in the summer polar mesosphere over Andenes (69°N, 16°E), Norway, *Geophys. Res. Lett.*, *15*, 1263–1266, 1988.

Sutherland, B. R., Finite-amplitude internal wavepacket dispersion and breaking, *J. Fluid Mech.*, *429*, 343–380, 2001.

Swenson, G. R., and A. Z. Liu, A model for calculating acoustic gravity wave energy and momentum flux in the mesosphere from OH airglow, *Geophys. Res. Lett.*, *25*, 477–480, 1998.

Swenson, G. R., and S. B. Mende, OH emission and gravity waves (including a breaking wave) in all-sky imagery from Bear Lake, UT, *Geophys. Res. Lett.*, *21*, 2239–2242, 1994.

Taylor, M. J., D. C. Fritts, and J. R. Isler, Determination of an unusual pattern of short period gravity waves imaged during ALOHA-93, *Geophys. Res. Lett.*, *22*, 2837–2840, 1995.

Vadas, S. L., and D. C. Fritts, Gravity wave radiation and mean responses to local body forces in the atmosphere: Mean and gravity wave responses, *J. Atmos. Sci.*, *58*, 2249–2279, 2001.

Vadas, S. L., D. C. Fritts, and M. J. Alexander, Mechanism for the generation of secondary waves in wave breaking regions, *J. Atmos. Sci.*, in press, 2002.

Walterscheid, R. L., J. H. Hecht, R. A. Vincent, I. M. Reid, J. Woithe, and M. P. Hickey, Analysis and interpretation of airglow and radar observations of quasi-monochromatic gravity waves in the upper mesosphere and lower thermosphere over Adelaide, Australia (35°S, 138°E), *J. Atmos. Solar-Terres. Phys.*, *61*, 461–478, 1999.

Yamada, Y., H. Fukunishi, T. Nakamura, and T. Tsuda, Breaking of small-scale gravity wave and transition to turbulence observed in OH airglow, *Geophys. Res. Lett.*, *28*, 2153–2156, 2001.

———————————

D. C. Fritts and S. L. Vadas, NWRA/ CoRA Division, 3380 Mitchell Lane, Boulder, CO 80301, USA. (dave@co-ra.com)

Yoshinori Yamada, Department of Geophysics, Tohoku University, Sendai, Japan.